Desalination and Water Treatment
www.deswater.com

doi: 10.5004/dwt.2019.24357

157 (2019) 372–382
July

Comparison of scale formation between inside-out and outside-in hollow fiber membrane distillation (MD) modules when concentrating hyper saline feed solutions

Youngkyu Park, Yongjun Choi, Jihyeok Choi, Jaehyun Ju, Dongha Kim, Sangho Lee*

School of Civil and Environmental Engineering, Kookmin University, 77 Jeongneung-ro, Seoungbuk-gu, Seoul 02707, Republic of Korea, Tel. +82-2-910-4529; Fax: +82-2-910-4939; email: sanghlee@kookmin.ac.kr (S. Lee)

Received 24 October 2018; Accepted 5 May 2019

ABSTRACT

This study focused on the comparison of inside-out or outside-in membrane distillation (MD) modules under the conditions where fouling due to scale formation occurs. Experiments were carried out using a laboratory-scale direct contact MD setup. Synthetic feed water containing NaCl of 200,000 mg/L and $CaSO_4$ of 2,000 mg/L was used for accelerated fouling tests. In-house MD mini modules were fabricated and operated either in the inside-out or outside-in modes. Results showed that the initial flux of the inside-out MD module was slightly higher than the outside-in MD module under no fouling conditions. The temperature difference was maintained at 40°C (feed inlet: 60°C; distillate: 20°C). The flow rate of the feed was the same as that of the distillate, which was 0.4 L/min. The average flux values of the inside-out and outside-in modes were, approximately, 1.56 and 1.42 kg/m^{2}h, respectively. However, a more rapid decline of flux due to scale formation occurred in the inside-out MD modules compared with the outside-in MD modules under the same operating condition. The blocking coefficient was initially very low and suddenly increased after the volume of concentration factor (VCF) of 1.35 in the case of the inside-out mode. The blocking coefficient started to increase after the VCF of 1.75 in the case of the outside-in mode. Different mechanisms for scale formation in the inside-out and outside-in modes were suggested to elucidate the results of fouling tests, which were also supported by the scanning electron microscope analysis.

Keywords: Membrane distillation (MD); Hollow fiber membrane; Scale formation; Inside-out and outside-in MD modules

1. Introduction

As water shortage due to imbalance between available water resources and water demand has become serious, many countries have been searching for novel technologies to supply sustainable sources of fresh water [1,2]. One of the promising technologies is seawater reverse osmosis (SWRO) desalination that can produce fresh water from saline water [3–5]. However, SWRO requires a substantial amount of electricity and may not be affordable since cost of the electricity is high. Accordingly, there is an ongoing need for desalination techniques that do not rely on electrical energy generated from fossil fuels. In this context, membrane distillation (MD) has drawn attention as a desalination technology capable of reducing the electricity consumption by using thermal energy [6–9]. Since MD may be operated under lower feed temperature than multistage flash or multi-effect distillation, it allows the use of low grade heat sources such as solar thermal energy or waste heat [10–14].

Current applications of MD have been attempted in small scales, which have limited impacts on desalination industry. One of the reasons is that most MD modules in

* Corresponding author.

Presented at the EDS conference on Desalination for the Environment: Clean Water and Energy, 3–6 September 2018, Athens, Greece

1944-3994/1944-3986

commercial or pilot scales are produced using flat sheet membranes. Although they are advantageous in small-scale applications, it is difficult to scale up using such membrane modules due to relatively low packing density of the membranes [15]. Recently, hollow fiber MD modules have been also developed in commercial scales, which have potential for large-scale applications for desalination as well as SWRO brine treatment [16,17]. Compared with flat sheet MD modules, hollow fiber MD modules have higher packing density and lower module cost per membrane area [17–19].

In hollow fiber MD modules, there are several design and operational factors influencing the process efficiency and one of them is the selection of flow direction. Unlike flat-sheet MD modules, hollow fiber MD modules may be operated either inside-out or outside-in modes [20]. Preliminary works revealed that their performances are similar under no fouling conditions [17,21,22]. Nevertheless, little information is available on the performances of such modules under severe fouling conditions [23]. The inorganic fouling may deposit on the membrane surface and block the membrane pores and it has a profound effect on MD flux [24–26]. The scale formation gives additional thermal and hydraulic resistances, which depend on the characteristics of the scale formation such as porosity and thickness. The formation of fouling layer reduces the temperature difference across the membrane or an increase in temperature polarization, which translates to lesser driving force [23].

Thus, this study focused on the comparison of inside-out or outside-in MD modules under the conditions where fouling due to scale formation occurs. Experiments were carried out using in-house MD modules in the direct contact MD mode. Accelerated fouling tests were done using synthetic feed solution containing high concentrations of NaCl and $CaSO_4$ [20]. The results were compared to suggest different mechanisms of fouling due to scale formation in the two modes.

2. Material and methods

2.1. Membrane module

Detailed specifications of the membrane modules are listed in Table 1. Fig. 1a shows the photograph of the hollow fiber module, and SEM images of cross-sectional membrane structure before MD experiments are in Fig. 1b. The effect of the membrane structure was not considered in this study.

Table 1
Summary of membrane specifications

Parameters	Specifications
Membrane type	Hollow fiber membrane
Membrane material	Hydrophobic polyvinylidene fluoride (PVDF)
Fiber inside diameter (m)	8×10^{-4}
Fiber outside diameter (m)	12×10^{-4}
Pore size (m)	1×10^{-7}
Porosity (%)	80
Module diameter (m)	0.04
Module length (m)	0.18
Effective membrane area (m^2)	0.0188

2.2. Experimental setup

Experiments were carried out in a bench-scale direct contact membrane distillation (DCMD) system, which is schematically illustrated in Fig. 1c. The temperature of feed solution was automatically controlled by a heat with a thermometer. The feed flow and distillate flow rates were adjusted from 0.2 to 0.4 L/min. The feed inlet temperature had a range from 50°C to 70°C. The permeate temperature was fixed at 20°C by a heat exchanger connected to a cooler. The temperature difference between the feed and distillate (ΔT) was ranged from 30°C to 50°C. The distillate flux was calculated by measuring the volume of distillate water using an electronic balance (OHAUS, USA). Two gear pumps (Cole-Parmer, USA) were used to recirculate the feed and distillate. The flow rates were monitored using flow meters (Dwyer, USA), which were placed at the inlet side of the module.

The flow directions for the inside-out and outside-in modes are illustrated in Fig. 2. In the inside-out mode, the feed water was supplied to the lumen side and the distillate water flowed through the shell side. In the outside-in mode, the feed water was supplied to the shell side and the distillate water flowed through the lumen side.

2.3. Feed solution

To examine fouling behaviors of the MD membranes, the feed solution was prepared using NaCl of 200,000 mg/L and $CaSO_4$ of 2,000 mg/L. All reagents were purchased from Sigma-Aldrich (St. Louis, MO). Table 2 shows the solubility limits of NaCl and $CaSO_4$ at feed temperatures. The solubility of $CaSO_4$ decreases with the increase of temperature.

2.4. Experimental procedures

2.4.1. Accelerated fouling tests and calculation of blocking coefficient (β)

In order to compare fouling propensity in the two operation modes, a series of MD experiments were carried out using the feed water. The effect of flow rate on flux was also examined in the two operation modes. All the tests were done in the batch operation mode. The degree of concentration is expressed as the volume of concentration factor (VCF), which is defined as:

$$\mathrm{VCF} = \frac{V_0}{V_0 - V_p} \tag{1}$$

where V_0 is the initial quantity of feed volume and V_p is the cumulative permeate production. Accordingly, the changes in flux were compared as a function of VCF.

It has been reported that the progress of membrane fouling due to scale formation is caused by the blockage of

(a)

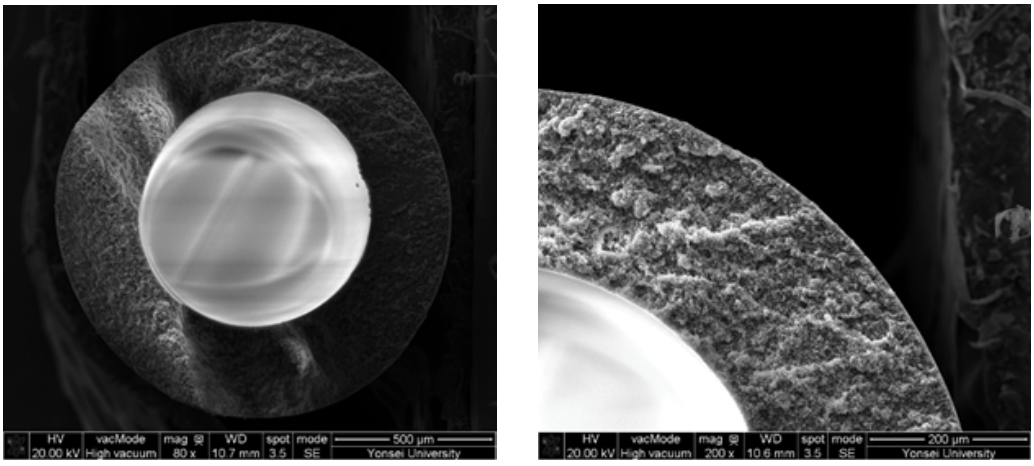

(b)

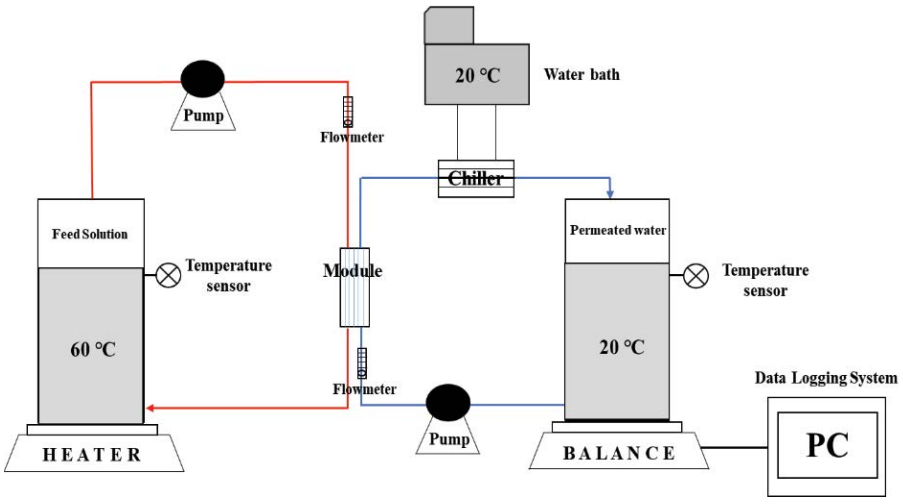

(c)

Fig. 1. (a) Hollow fiber DCMD module, (b) SEM images of cross-sectional membrane structure before MD experiments, and (c) schematic diagram of laboratory DCMD experimental system.

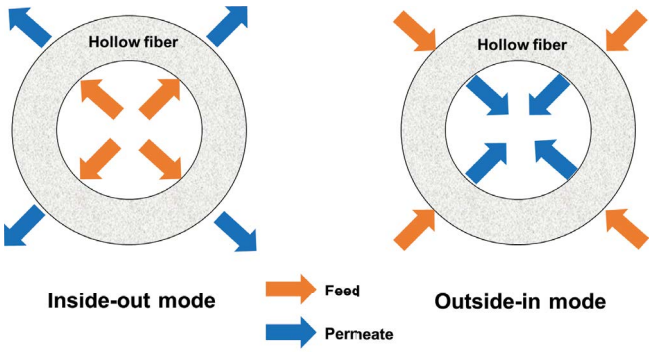

Fig. 2. Flow directions in (a) inside-out mode and (b) outside-in mode.

Table 2
Solubility limits of NaCl, $CaSO_4$ at feed temperatures

Feed solution	Solubility limit (mg/mL)		
	Feed temperature of 50°C	Feed temperature of 60°C	Feed temperature of 70°C
NaCl	367	370	375
$CaSO_4$	2.07	2.01	1.93

membrane surface by the deposition of crystals formed from either surface crystallization or bulk crystallization [16,27–30]. Accordingly, the following equations were applied to describe the progress of fouling [23]:

$$J = B(\Delta p)\frac{A_m - A_b}{A_m} = B(\Delta p)(1-\beta) \tag{2}$$

$$\Delta p = p_0(\mathrm{VCF}) \tag{3}$$

where J is the distillate flux; B is the water permeability of MD membrane; A_m is the membrane area; A_b is the membrane area blocked by scales; Δp is the effective vapor pressure difference between the feed and distillate [31]; and β is the blocking coefficient given by A_b/A_m. These equations were developed to describe fouling due to scale formation in membrane systems. They are based on the assumption that the growth of inorganic scales blocks the membrane surface, thereby reducing the effective membrane area [23].

Accordingly, β is calculated using the ratio of flux at a given VCF to the initial flux (J_0):

$$\beta = 1 - \frac{J}{B(p_0(\mathrm{VCF}))} = 1 - \frac{J}{J_0} \tag{4}$$

The physical meaning of β is the ratio of the membrane area which is blocked by the crystals. If β approaches to 1.0, the membrane is completely blocked, implying serious fouling. As VCF increases, the salt concentration increases, leading to an increased rate of crystallization. Therefore, β rapidly increases with VCF during the MD operation.

2.4.2. Field emission scanning electron microscopy (FE-SEM)

After each MD experiment, the membrane was taken out from the module. Then, it was completely dried after washing with distilled water and mounted on the flat stubs after coated by platinum. The field emission scanning electron microscopy (FE-SEM) was used to examine the membrane surface.

2.4.3. Measurement of the pressure drop

Before the start of the experiment, the pressure drop of the MD modules was measured in the inside-out and the outside-in mode. After the fouling experiments, the pressure drops were measured again. They were measured in the flow rates of 0.40 and 0.20 L/min, respectively.

3. Results and discussion

3.1. No fouling conditions

The pure water flux in the inside-out mode was compared with that in the outside-in mode as shown in Fig. 3. The temperature difference was maintained at 40°C (feed inlet: 60°C; distillate: 20°C). The flow rate of the feed was same as that of the distillate, which was 0.4 L/min. The average flux values of the inside-out and outside-in modes were approximately 1.56 and 1.42 kg/m²h, respectively. It is evident that the flux in the inside-out mode was slightly higher than that of the outside-in mode under no fouling conditions.

This may be attributed to the difference in hydrodynamic conditions between the two modes. Although the feed flow rates were same, the crossflow velocities between the two modes were different due to the different cross section area. Therefore, the Reynolds numbers should be also different. The crossflow velocities and the Reynolds numbers for the inside-out and outside-in modes can be calculated using the following equations [32]:

$$u_i = \frac{Q_{\mathrm{feed}}}{A_i} = \frac{Q_{\mathrm{feed}}}{\frac{n_f \pi d_i^2}{4}} \tag{5}$$

$$\mathrm{Re}_i = \frac{\rho u_i d_i}{\mu} = \frac{\rho Q_{\mathrm{feed}} d_i}{\frac{\mu n_f \pi d_i^2}{4}} \tag{6}$$

$$u_o = \frac{Q_{\mathrm{feed}}}{A_o} = \frac{Q_{\mathrm{feed}}}{\left(\frac{\pi d_m^2}{4} - \frac{n_f \pi d_o^2}{4}\right)} \tag{7}$$

$$\mathrm{Re}_o = \frac{\rho u_o D_e}{\mu} = \frac{\rho Q_{\mathrm{feed}} D_e}{\mu A_o} = \frac{\rho Q_{\mathrm{feed}} D_e}{\mu\left(\frac{\pi d_m^2}{4} - \frac{n_f \pi d_o^2}{4}\right)} \tag{8}$$

$$D_e = \frac{4\left(P_t^2 - \frac{\pi d_o^2}{4}\right)}{\pi d_o} \tag{9}$$

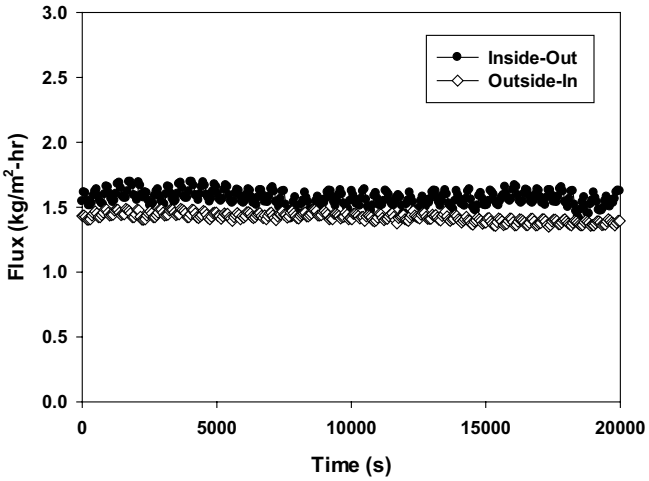

Fig. 3. Comparison of pure water flux between inside-out and outside-in operations under no fouling condition. (symbols: ●: inside-out; ◇: outside-in; operating conditions: feed solution: distilled water; feed temperature: 60°C; distillate temperature: 20°C; flow rate; 0.4 L/min).

where Re_i is the Reynolds number for the inside-out mode; Re_o is the Reynolds number for the outside-in mode; ρ is the density of the feed solution; m is the viscosity of the feed solution, u_i is the crossflow velocity of the feed in the inside-out mode, u_o is the crossflow velocity of the feed in the outside-in mode; Q_{feed} is the feed flow rate; d_i is the fiber inner diameter; d_o is the fiber outer diameter; d_m is the inner diameter of the module; A_i is the cross section area for feed flow in the inside-out mode; A_o is the cross section area for feed flow in the outside-in mode; D_e is the equivalent diameter in the inside-out mode; and P_i is the tube pitch.

Table 3 summarizes the calculated values for the crossflow velocities, viscosity and feed concentration in the inside-out and outside-in modes. Table 4 shows Reynolds numbers in the inside-out and outside-in modes. Since the viscosity of the water changes with the temperature, the Reynolds numbers were calculated at three different feed temperatures [31]. The crossflow velocities in the inside-out mode are much higher than those in the outside-in mode under all cases. The Reynolds numbers were also higher in the inside-out mode than in the outside-in mode. It is expected that the degree of the temperature polarization in the inside-out mode is lower than that in the outside-in mode due to the difference in the Reynolds numbers [33]. Accordingly, it can be concluded that the pure water flux in the inside-out mode is higher than that in the outside-in mode for our hollow module under same feed flow rate.

3.2. Effect of operation mode on flux decline due to scale formation

A series of MD experiments were performed using the feed water to compare the fouling propensities between the inside-out and the outside-in modes. The changes in flux at the temperature difference of 40°C and the flow rate of 0.4 L/min are shown in Fig. 4a. Although the initial flux was slightly higher in the inside-out mode than the outside-in mode, a more rapid flux decline was observed in the inside-out mode. As depicted in Fig. 4b, the blocking coefficient was initially very low and suddenly increased after the VCF of 1.35 in the case of the inside-out mode. However,

Table 3
Comparison of calculated crossflow velocities, viscosity and feed concentration

Operation mode	Flow rate (L/min)	Crossflow velocity (m/s)	Viscosity (sec-Pa)			Feed concentration (ppm) (average concentration of initial value and critical value)		
			Feed temperature of 50°C	Feed temperature of 60°C	Feed temperature of 70°C	Feed temperature of 50°C	Feed temperature of 60°C	Feed temperature of 70°C
Inside-out	0.4	0.829	0.001005	0.000861	0.000740	235,000	235,000	230,000
	0.2	0.415	0.001018	0.000873	0.000740	240,000	240,000	230,000
Outside-in	0.4	0.0074	0.001061	0.000955	0.000800	256,000	275,000	260,000
	0.2	0.0037	0.001070	0.000992	0.000800	259,000	290,000	260,000

Table 4
Comparison of calculated Reynolds numbers

Operation mode	Flow rate (L/min)	Reynolds number		
		Feed temperature of 50°C	Feed temperature of 60°C	Feed temperature of 70°C
Inside-out	0.40	767	890	1,027
	0.20	380	441	514
Outside-in	0.40	279	312	367
	0.20	139	152	177

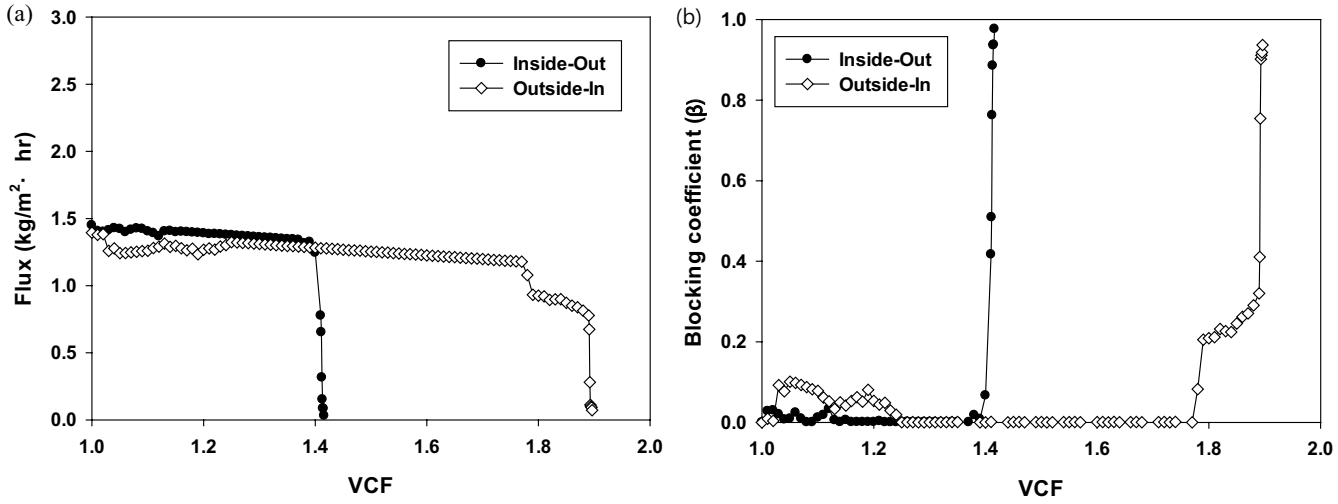

Fig. 4. Dependence of flux and blocking coefficient on VCF during the MD experiments in the inside-out and outside-in modes. (a) Flux and (b) blocking coefficient (symbols: ●: inside-out; ◇: outside-in; operating conditions: feed solution: distilled water; feed temperature: 60°C; distillate temperature: 20°C; flow rate; 0.4 L/min).

the blocking coefficient started to increase after the VCF of 1.75 in the case of the outside-in mode. It is evident from the results that the inside-out mode operation is more sensitive to fouling due to scale formation.

Fig. 5a shows the flux behaviors at the temperature difference of 40°C and the flow rate of 0.2 L/min. As the feed flow range decreased from 0.4 to 0.2 L/min, the initial flux in the inside-out and outside-in modes was reduced from 1.45 to 0.941 kg/m^{2}h and from 1.4 to 0.915 kg/m^{2}h, respectively. It is clear that the flow rate is an important factor influencing the initial flux of the hollow fiber MD. Similar to the previous case, the flux decline in the inside-out mode is more serious than in the outside-in mode. The blocking coefficients began to increase from the VCF of 1.4 in the inside-out mode and the VCF of 1.9 in the outside-in mode. Again, it is evident that the fouling due to scale formation is more serious in the inside-out mode than the outside-in mode regardless of the flow rates.

After the MD experiments, the modules were disassembled and visually examined to compare the differences between the two modes. In the inside-out mode, there were substantial amounts of scales attaching to the inlet channel of the module as depicted in Fig. 6a. However, in the outside-in mode, a large amount of scales was found on the surface of the fibers as demonstrated in Fig. 6b. To further examine the scales on the membranes, SEM was applied as shown in Fig. 7. The inlet section and the middle section were observed using SEM in the two modes. As shown in Fig. 7a, scales were found inside the fibers in the inlet section after the MD operation in the inside-out mode. The fiber seems to

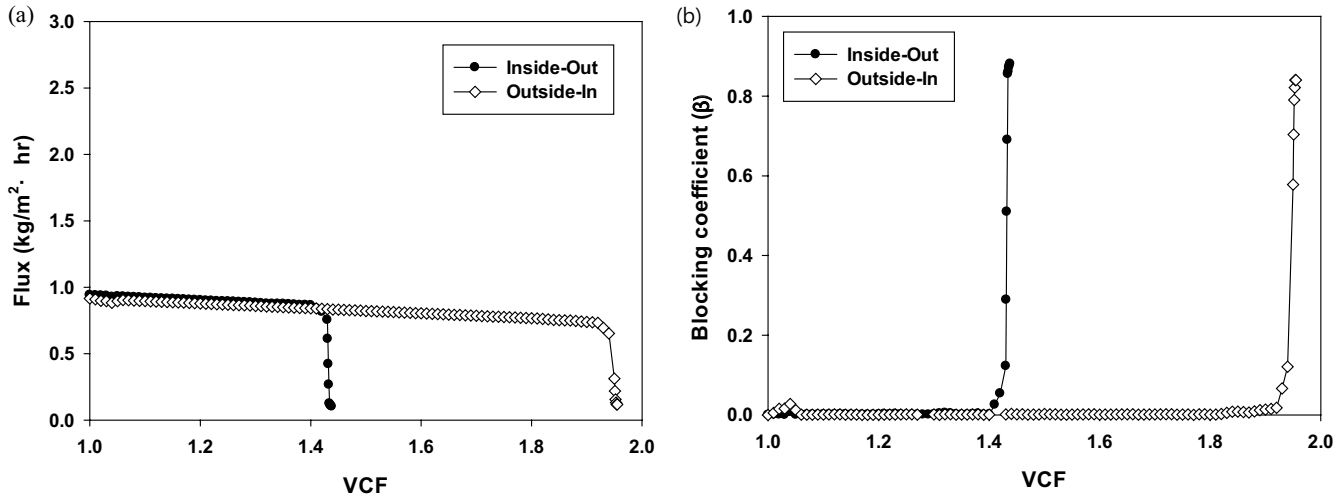

Fig. 5. Dependence of flux and blocking coefficient on VCF during the MD experiments in the inside-out and outside-in modes. (a) Flux and (b) blocking coefficient (symbols: ●: inside-out; ◇: outside-in; operating conditions: feed solution: distilled water; feed temperature: 60°C; distillate temperature: 20°C; flow rate; 0.2 L/min).

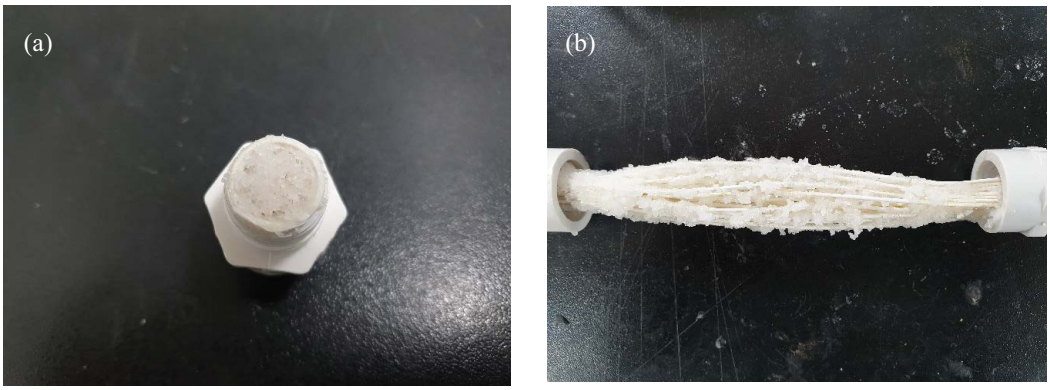

Fig. 6. Photographs of the membrane module after MD experiments (a) inside-out mode and (b) outside-in mode.

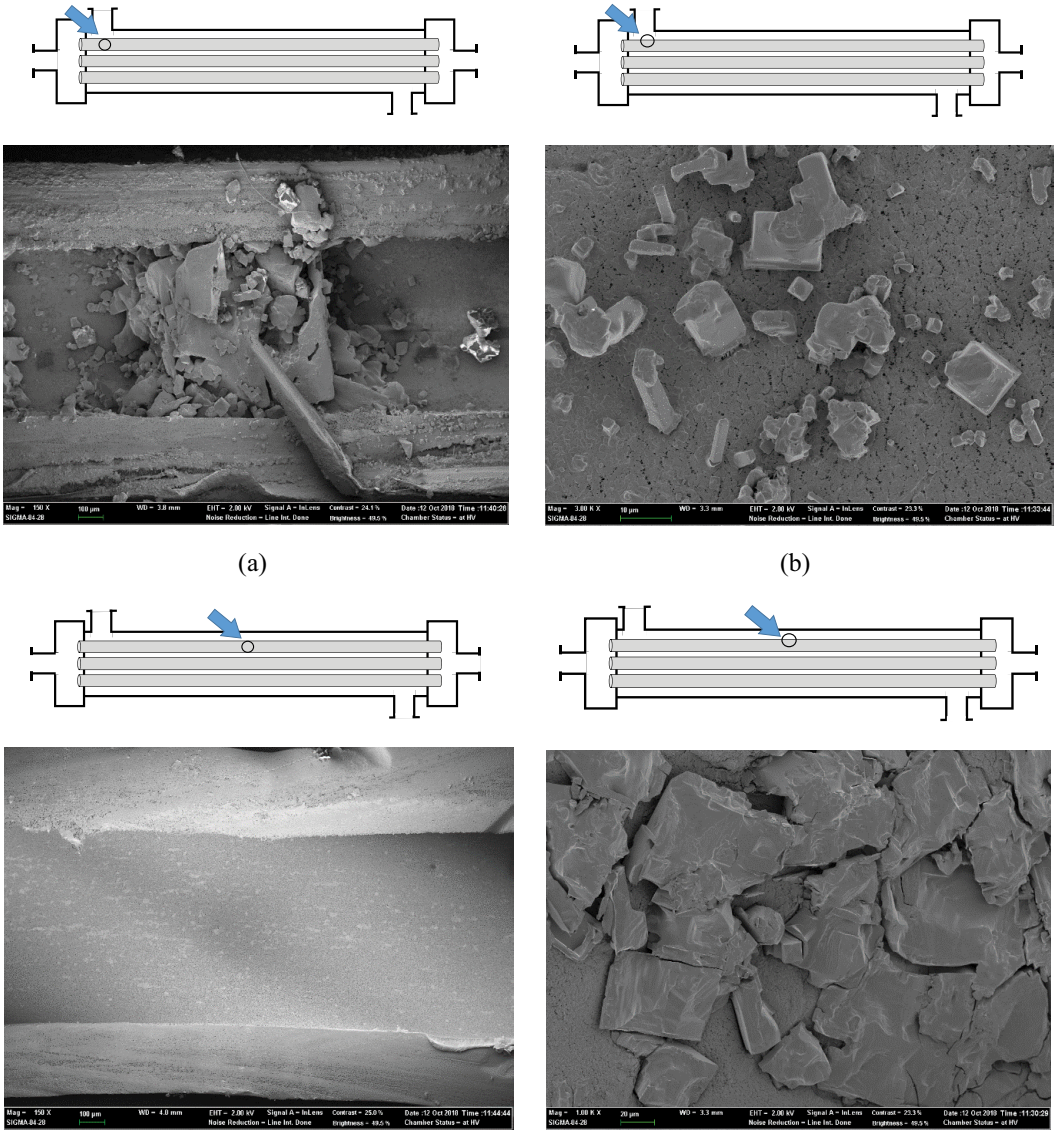

Fig. 7. SEM images of membranes after MD experiments (a) inside of membrane inlet section in the inside-out mode, (b) surface of membrane inlet section in the outside-in mode, (c) inside of membrane middle section in the inside-out mode, and (d) surface of membrane middle section in the outside-in mode.

be completely clogged by the scales in this case. However, no scales were observed in the middle section (Fig. 7c), suggesting that the inlet of the fiber is blocked and thus feed water did not enter into the middle section. On the other hand, the scales were found not only in the inlet section (Fig. 7b) but also in the middle section (Fig. 7d) in the case of the outside-in mode.

Based on the results of fouling tests (Figs. 4 and 5) and SEM analysis (Fig. 7), the mechanisms for the scale formation in the inside-out and outside-in modes were suggested. As illustrated in Figs. 8a and b, the scale formation in the inside-out mode mainly occurs near the inlet section of the fibers. During the MD operation, scales are generated through the bulk crystallization and enter in the fibers, thereby clogging the fibers. Although the remaining part of the fiber may be clean without scale deposits, it may not be used for water production because the feed water cannot enter. A relatively small amount of crystals can block the fibers and thus the flux decline due to scale formation rapidly occurs. On the other hand, the scale formation in the outside-in mode occurs on the outer surface of the fibers. Due to low crossflow velocity and Reynolds number, the condition is favorable for surface crystallization. However, the blockage of the whole membrane surface by the surface crystallization requires a certain amount of time. Accordingly, it is likely that the flux decline is slower in the outside-in mode than the inside-out mode.

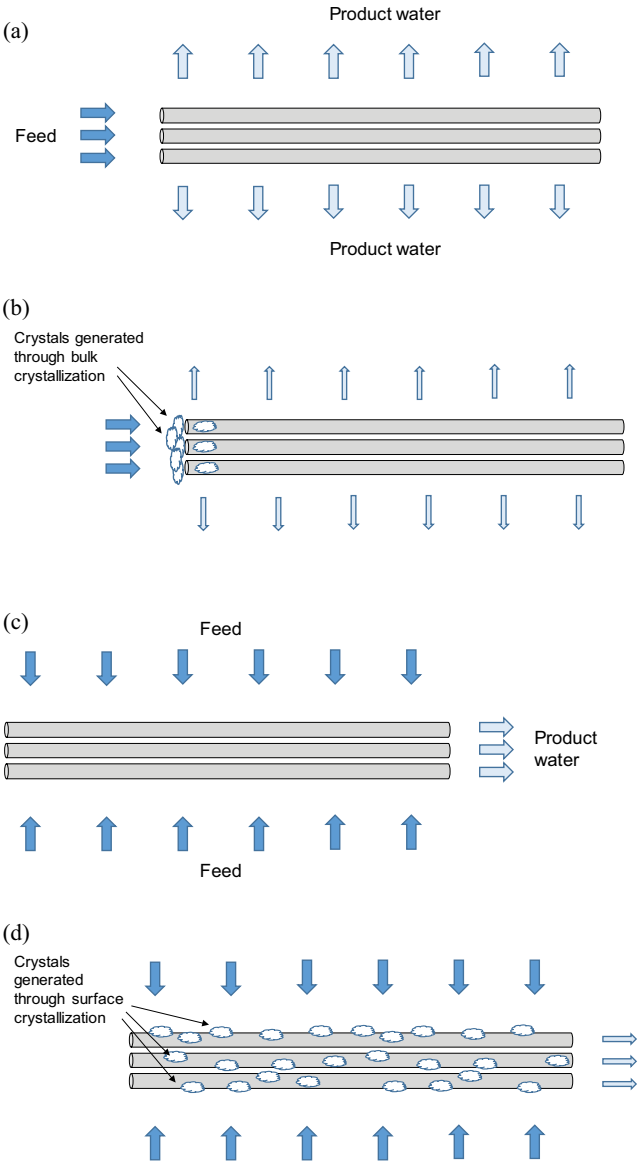

Fig. 8. Proposed mechanisms of scale formation in inside-out and outside-in modes: (a) inside-out without scale formation, (b) inside-out with scale formation, (c) outside-in without scale formation, and (d) outside-in with scale formation.

If the membrane fibers were clogged by the scales in the inside-out mode, the pressure drop of the module should have increased after the MD experiment. As demonstrated in Table 5, in the case of the inside-out mode, the inlet pressure increased from 0.04 to 0.33 bar at the flow rate of 0.40 L/min and from 0.02 to 0.16 bar at the flow rate of 0.20 L/min. However, it did not change before and after the experiment in the case of the outside-in mode. This is an evidence supporting the mechanisms proposed in Fig. 8.

3.3. Effect of temperature difference

The temperature difference is one of the most important factors influencing the results of MD operation. Accordingly, the effect of the temperature differences was also investigated in the two operation modes. First, the temperature difference was increased to 50°C. In Fig. 9, the flux and blocking coefficient are illustrated as a function of VCF at the temperature difference of 50°C and the flow rate of 0.4 L/min. Compared with the previous case (Fig. 4), the initial fluxes were higher, but the flux declines were also more serious. The blocking coefficients gradually increased from the beginning and then suddenly rose at the VCF of 1.3 in the inside-out mode and 1.6 in the outside-in mode. Similar results were obtained when the temperature difference of 50°C and the feed flow rate was 0.2 L/min, as shown in Fig. 10.

The results of MD experiments at the temperature difference of 30°C are illustrated in Figs. 11 and 12. The initial flux was reduced with a decrease in the temperature difference. The rates of flux decline were lower than the cases with the temperature difference of 50°C but similar to the cases with the temperature difference of 40°C. This implies that the flux decline due to scale formation cannot be properly managed by reducing the temperature difference.

Regardless of the temperature differences, the fouling propensity in the inside-out mode was higher than that in the outside-in mode. But there were slight differences depending on the temperature conditions. When the temperature difference was higher (Fig. 9a), the difference in the flux between the two modes became larger. On the other hand, the difference became smaller at the lower temperature difference (Fig. 11a). This suggests that the fouling in the inside-out mode is accelerated at higher temperature differences.

To further investigate the scaling phenomena in inside-out and outside-in, the critical VCF values, which are defined as the VCF to result in a rapid decrease in flux, were compared with the corresponding saturation degree and Reynolds number (Table 6). The saturation degrees for

Table 5
Measurement of pressure drop along with the module before and after scale formation

Operation mode	Flow rate (L/min)	Initial pressure of feed inlet (bar)	Initial pressure of feed outlet (bar)	Pressure of feed inlet after scale formation (bar)	Pressure of feed outlet after scale formation (bar)
Inside-out	0.40	0.04	0.03	0.33	0.01
	0.20	0.02	0.01	0.16	0.01
Outside-in	0.40	0.06	0.02	0.06	0.02
	0.20	0.03	0.01	0.03	0.01

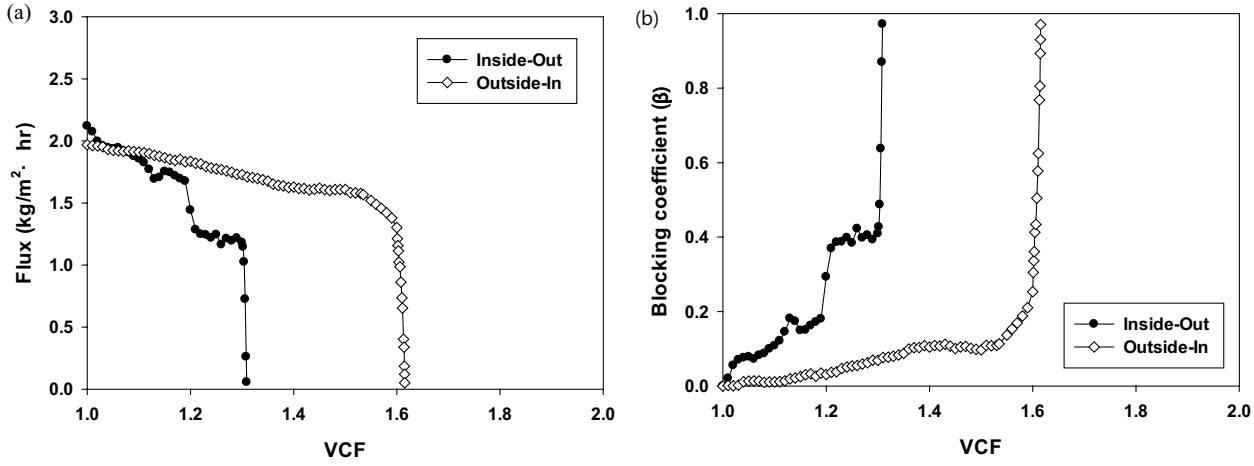

Fig. 9. Dependence of flux and blocking coefficient on VCF during the MD experiments in the inside-out and outside-in modes. (a) Flux and (b) blocking coefficient (symbols: ●: inside-out; ◇: outside-in; operating conditions: feed solution: distilled water; feed temperature: 70°C; distillate temperature: 20°C; flow rate; 0.4 L/min).

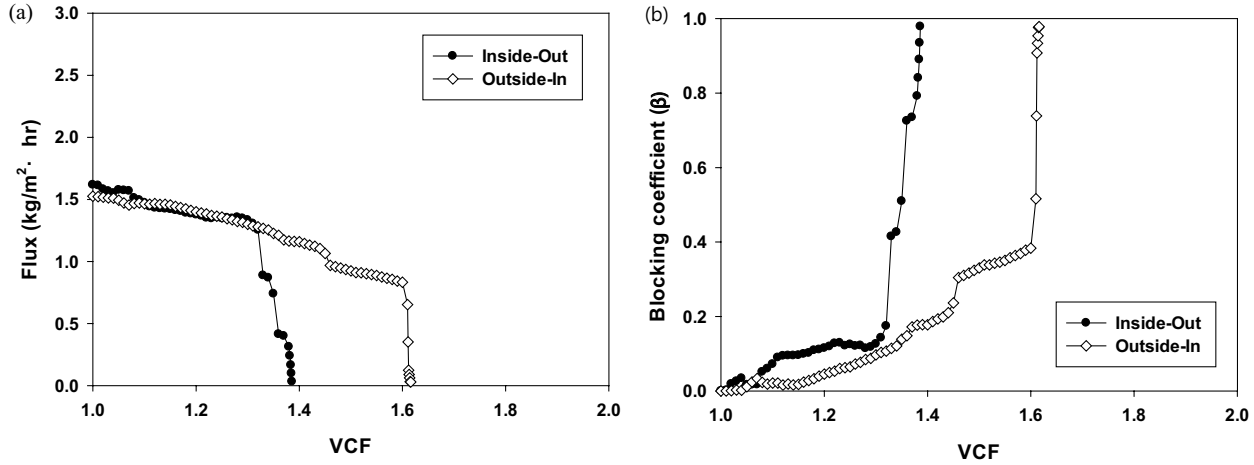

Fig. 10. Dependence of flux and blocking coefficient on VCF during the MD experiments in the inside-out and outside-in modes. (a) Flux and (b) blocking coefficient (symbols: ●: inside-out; ◇: outside-in; operating conditions: feed solution: distilled water; feed temperature: 70°C; distillate temperature: 20°C; flow rate; 0.2 L/min).

NaCl and $CaSO_4$ in the inside-out module range from 0.69 to 0.76 and from 1.26 to 1.39, respectively. On the other hand, the saturation degrees for NaCl and $CaSO_4$ in the outside-in module range from 0.84 to 1.03 and from 1.50 to 1.89, respectively. In both modules, the Reynolds number was not related with the critical VCF values. This suggests that the inside-out module is more sensitive to scale formation than the outside-in module regardless of their hydrodynamic conditions in the modules. Together with the results in Table 5, it can be concluded that the different critical VCF between inside-out and outside-in modules is attributed to the clogging of fiber inlets in the inside-out module.

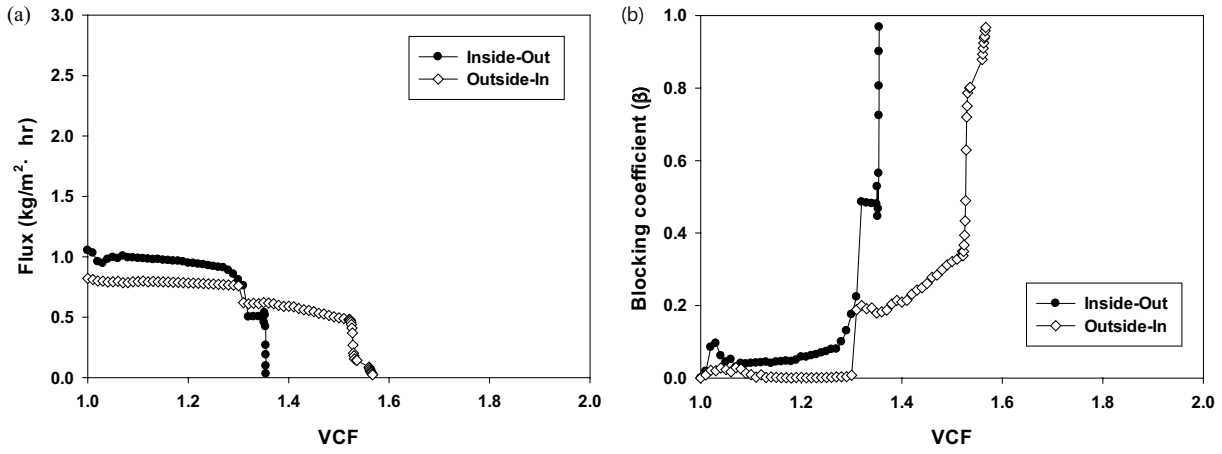

Fig. 11. Dependence of flux and blocking coefficient on VCF during the MD experiments in the inside-out and outside-in modes. (a) flux and (b) blocking coefficient (symbols: ●: inside-out; ◇: outside-in; operating conditions: feed solution: distilled water; feed temperature: 50°C; distillate temperature: 20°C; flow rate; 0.4 L/min).

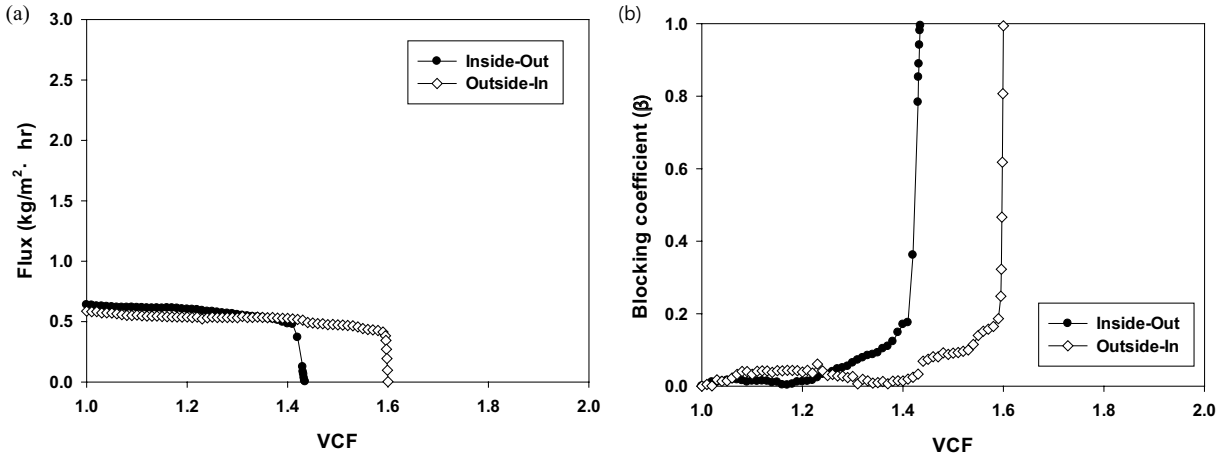

Fig. 12. Dependence of flux and blocking coefficient on VCF during the MD experiments in the inside-out and outside-in modes. (a) flux and (b) blocking coefficient (symbols: ●: inside-out; ◇: outside-in; operating conditions: feed solution: distilled water; feed temperature: 50°C; distillate temperature: 20°C; flow rate; 0.2 L/min).

Table 6
Summary of critical VCF values under various conditions

Feed temperature (°C)	Operation mode	Flow rate (L/min)	Critical VCF	Saturation degree		Reynolds number
				NaCl	$CaSO_4$	
50	Inside-out	0.4	1.3	0.71	1.26	767
		0.2	1.4	0.76	1.35	380
	Outside-in	0.4	1.55	0.84	1.50	279
		0.2	1.6	0.87	1.55	139
60	Inside-out	0.4	1.4	0.76	1.39	890
		0.2	1.4	0.76	1.39	441
	Outside-in	0.4	1.75	0.95	1.74	312
		0.2	1.9	1.03	1.89	152
70	Inside-out	0.4	1.3	0.69	1.35	1,027
		0.2	1.3	0.69	1.35	514
	Outside-in	0.4	1.6	0.85	1.66	367
		0.2	1.6	0.85	1.66	177

4. Conclusions

In this study, different fouling behaviors of the hollow fiber MD membranes between the inside-out and the outside-in modes were analyzed in a bench-scale DCMD system. The following conclusions were drawn:

- Without fouling, the flux in the inside-out mode was slightly higher than that in the outside-in mode. This is attributed to a lower degree of temperature polarization in the inside-out mode operation caused by higher crossflow velocity and Reynolds number.
- However, a more severe fouling due to scale formation occurred in the inside-out mode compared with that in the outside-in mode. It appears that the scale formation in the inside-out mode mainly occurs near the inlet section of the fibers, leading to clogging of the fibers. On the other hand, the scale formation in the outside-in mode seems to occur on the outer surface of the fibers.
- Regardless of the flow rates and temperature differences, the fouling due to scale formation was more serious in the inside-out mode than the outside-in mode. However, the fouling in the inside-out mode became higher at higher temperature differences compared with the outside-in mode.

Acknowledgment

This work was supported by the Korea Institute of Energy Technology Evaluation and Planning (KETEP) and the Ministry of Trade, Industry &Energy (MOTIE) of the Republic of Korea (No. 20183010141130).

References

[1] X. Zheng, D. Chen, Q. Wang, Z.X. Zhang, Seawater desalination in China: retrospect and prospect, Chem. Eng. J., 242 (2014) 404–413.
[2] B.C. Ferguson, N. Frantzeskaki, R.R. Brown, A strategic program for transitioning to a water sensitive city, Landscape Urban Plann., 117 (2013) 32–45.
[3] M.P. Shahabi, A. McHugh, M. Anda, G. Ho, Comparative economic and environmental assessments of centralised and decentralised seawater desalination options, Desalination, 376 (2015) 25–34.
[4] V. Martinez-Alvarez, B. Martin-Gorriz, M. Soto-Garcia, Seawater desalination for crop irrigation — A review of current experiences and revealed key issues, Desalination, 381 (2016) 58–70.
[5] V.G. Gude, Desalination and sustainability - an appraisal and current perspective, Water Res., 89 (2016) 87–106.
[6] G. Amy, N. Ghaffour, Z.Y. Li, L. Francis, R.V. Linares, T. Missimer, S. Lattemann, Membrane-based seawater desalination: present and future prospects, Desalination, 401 (2017) 16–21.
[7] D.L. Zhao, S.C. Chen, C.X. Guo, Q.P. Zhao, X.M. Lu, Multifunctional forward osmosis draw solutes for seawater desalination, Chin. J. Chem. Eng., 24 (2016) 23–30.
[8] N. Ghaffour, J. Bundschuh, H. Mahmoudi, M.F.A. Goosen, Renewable energy-driven desalination technologies: a comprehensive review on challenges and potential applications of integrated systems, Desalination, 356 (2015) 94–114.
[9] A. Subramani, J.G. Jacangelo, Emerging desalination technologies for water treatment: a critical review, Water Res., 75 (2015) 164–187.
[10] A. Alkhudhiri, N. Darwish, N. Hilal, Membrane distillation: a comprehensive review, Desalination, 287 (2012) 2–18.
[11] E. Drioli, A. Ali, F. Macedonio, Membrane distillation: recent developments and perspectives, Desalination, 356 (2015) 56–84.
[12] I. Hitsov, T. Maere, K. De Sitter, C. Dotremont, I. Nopens, Modelling approaches in membrane distillation: a critical review, Sep. Purif. Technol., 142 (2015) 48–64.
[13] M.A. Abu-Zeid, Y.Q. Zhang, H. Dong, L. Zhang, H.L. Chen, L. Hou, A comprehensive review of vacuum membrane distillation technique, Desalination, 356 (2015) 1–14.
[14] B.B. Ashoor, S. Mansour, A. Giwa, V. Dufour, S.W. Hasan, Principles and applications of direct contact membrane distillation (DCMD): a comprehensive review, Desalination, 398 (2016) 222–246.
[15] J. Koo, S. Lee, J.-S. Choi, T.-M. Hwang, Theoretical analysis of different membrane distillation modules, Desal. Wat. Treat., 54 (2015) 862–870.
[16] L. Fortunato, Y. Jang, J.-G. Lee, S. Jeong, S. Lee, T. Leiknes, N. Ghaffour, Fouling development in direct contact membrane distillation: non-invasive monitoring and destructive analysis, Water Res., 132 (2018) 34–41.
[17] Y. Choi, G. Naidu, S. Jeong, S. Vigneswaran, S. Lee, R. Wang, A.G. Fane, Experimental comparison of submerged membrane distillation configurations for concentrated brine treatment, Desalination, 420 (2017) 54–62.
[18] Y. Li, C. Jin, Y. Peng, Q. An, Z. Chen, J. Zhang, L. Ge, S. Wang, Fabrication of PVDF hollow fiber membranes via integrated phase separation for membrane distillation, J. Taiwan Inst. Chem. Eng., 95 (2018) 487–494.
[19] L. Cheng, Y. Zhao, P. Li, W. Li, F. Wang, Comparative study of air gap and permeate gap membrane distillation using internal heat recovery hollow fiber membrane module, Desalination, 426 (2018) 42–49.
[20] H. Cho, Y. Choi, S. Lee, Effect of pretreatment and operating conditions on the performance of membrane distillation for the treatment of shale gas wastewater, Desalination, 437 (2018) 195–209.
[21] J. Koo, J. Han, J. Sohn, S. Lee, T.-M. Hwang, Experimental comparison of direct contact membrane distillation (DCMD) with vacuum membrane distillation (VMD), Desal. Wat. Treat., 51 (2013) 6299–6309.
[22] H. Cho, Y.-J. Choi, S. Lee, J. Koo, T. Huang, Comparison of hollow fiber membranes in direct contact and air gap membrane distillation (MD), Desal. Wat. Treat., 57 (2016) 10012–10019.
[23] L.D. Tijing, Y.C. Woo, J.S. Choi, S. Lee, S.H. Kim, H.K. Shon, Fouling and its control in membrane distillation—A review, J. Membr. Sci., 475 (2015) 215–244.
[24] Q.M. Nguyen, S. Jeong, S. Lee, Characteristics of membrane foulants at different degrees of SWRO brine concentration by membrane distillation, Desalination, 409 (2017) 7–20.
[25] J.A. Sanmartino, M. Khayet, M.C. Garcia-Payo, H. El-Balcouri, A. Riaza, Treatment of reverse osmosis brine by direct contact membrane distillation: chemical pretreatment approach, Desalination, 420 (2017) 79–90.
[26] W.W. Zhong, H.Y. Li, Y. Ye, V. Chen, Evaluation of silica fouling for coal seam gas produced water in a submerged vacuum membrane distillation system, Desalination, 393 (2016) 52–64.
[27] H.-J. Oh, Y.-K. Choung, S. Lee, J.-S. Choi, T.-M. Hwang, J.H. Kim, Scale formation in reverse osmosis desalination: model development, Desalination, 238 (2009) 333–346.
[28] S. Lee, J. Kim, C.-H. Lee, Analysis of $CaSO_4$ scale formation mechanism in various nanofiltration modules, J. Membr. Sci., 163 (1999) 63–74.
[29] S. Lee, C.-H. Lee, Effect of operating conditions on $CaSO_4$ scale formation mechanism in nanofiltration for water softening, Water Res., 34 (2000) 3854–3866.
[30] J.-G. Lee, Y. Jang, L. Fortunato, S. Jeong, S. Lee, T. Leiknes, N. Ghaffour, An advanced online monitoring approach to study the scaling behavior in direct contact membrane distillation, J. Membr. Sci., 546 (2018) 50–60.
[31] M.H. Sharqawy, J.H. Lienhard, S.M. Zubair, Thermophysical properties of seawater: a review of existing correlations and data, Desal. Wat. Treat., 16 (2010) 354–380.
[32] S. Kakaç, H. Liu, Heat Exchangers: Selection, Rating and Thermal Design, CRC Press, Boca Raton, 2002.
[33] E. Jang, S.-H. Nam, T.-M. Hwang, S. Lee, Y. Choi, Effect of operating parameters on temperature and concentration polarization in vacuum membrane distillation process, Desal. Wat. Treat., 54 (2015) 871–880.